ELECTROCHEMISTRY

A green and sustainable strategy toward lithium resources recycling from spent batteries

Jing Xu[1], Yang Jin[1]*, Kai Liu[2]*, Nawei Lyu[1], Zili Zhang[1], Bin Sun[1], Qianzheng Jin[1], Hongfei Lu[1], Huajun Tian[3], Xin Guo[4], Devaraj Shanmukaraj[5], Hui Wu[6]*, Meicheng Li[2], Michel Armand[5]*, Guoxiu Wang[4]*

Recycling lithium from spent batteries is challenging because of problems with poor purity and contamination. Here, we propose a green and sustainable lithium recovery strategy for spent batteries containing $LiFePO_4$, $LiCoO_2$, and $LiNi_{0.5}Co_{0.2}Mn_{0.3}O_2$ electrodes. Our proposed configuration of "lithium-rich electrode || LLZTO@LiTFSI+P3HT || LiOH" system achieves double-side and roll-to-roll recycling of lithium-containing electrode without destroying its integrity. The LiTFSI+P3HT-modified LLZTO membrane also solves the H^+/Li^+ exchange problem and realizes a waterproof protection of bare LLZTO in the aqueous working environment. On the basis of these advantages, our system shows high Li selectivity (97%) and excellent Faradaic efficiency (≥97%), achieving high-purity (99%) LiOH along with the production of H_2. The Li extraction processes for spent $LiFePO_4$, $LiNi_{0.5}Co_{0.2}Mn_{0.3}O_2$, and $LiCoO_2$ batteries is shown to be economically feasible. Therefore, this study provides a previously unexplored technology with low energy consumption as well as high economic and environmental benefits to realize sustainable lithium recycling from spent batteries.

INTRODUCTION

Lithium is an essential element for Li-ion batteries (LIBs) owing to its low equivalent weight (6.94 g/Faraday) and very cathodic electrochemical potential (−3.04 V versus standard hydrogen electrode) (*1*, *2*). For the past few decades, LIBs for portable electronics, electric vehicles, and large-scale energy systems exhibit an exponential growth (*3*, *4*), leading to an increasing demand for lithium resources (*5*). As a typical alkali element, lithium is highly active and flammable, making it exist only in compounds in nature (*6*). In general, the natural lithium reserves are abundant and can be founded in lithium minerals (spodumene), salt lake brines, and seawater on the earth (*7*), but obstacles such as low lithium concentration, high extraction costs, and inconsistent product quality pose great difficulties during Li mining. For example, Li extraction from a spodumene must be specially designed as the mineral varies in chemical composition, hardness, and other properties. The present methods to extract Li from brines, which have low Li concentrations and range from 0.017 to 0.15% is based on evaporation and chemical precipitation that are highly time intensive (*8*). Besides, although the lithium reserves in the oceans seem unlimited, the low lithium concentration [0.180 parts per million (ppm)], poor maturity of the extraction techniques, and high production cost make seawater extraction unlikely in the near future (*9*). Thereby, sustainable strategies to recover Li element from the potentially valuable secondary resources is urgently needed to cope with the increasing Li demands.

As estimated, half a million tons of spent LIBs will be accumulated in 2025 (*10*). Considering the lithium content in spent LIBs [5 to 7 weight % (wt %)] is far higher than that in natural resources (*8*, *11*, *12*), spent LIBs are regarded as the most promising secondary lithium resources for the guaranteed supply of Li. However, according to the report of United Nations Environment Programme (*13*), the spent LIB recycling rate in the European Union is less than 5% and less than 1% of lithium is recycled. The lithium recycling technologies for spent LIBs mainly include pyrometallurgy, hydrometallurgy, biometallurgy, and electrochemical extraction (*12*, *14*–*17*). Pyrometallurgy usually applies high temperatures (>700°C) to calcinate the pretreated active materials and then dissolve the calcinated powders into water or solvent to separate lithium in the form of Li_2CO_3 (*18*, *19*). The shortcoming of this method for lithium recycling is that except for the calcination process, additional steps are required to separate Li_2CO_3. In addition, the pyrometallurgy method has high requirement on the calcination equipment and also has harmful gas emission, especially HF from the salt of the electrolyte. Hydrometallurgy is the most common method for lithium recycling (*20*). The pretreated active materials are first dissolved into acids or bases, followed by leaching to obtain Li^+ solutions for further lithium extraction. However, the conventional hydrometallurgy for lithium recycling requires a large volume of inorganic acids and lengthy extraction steps, which are expensive and environmentally unfriendly (*12*, *21*). Although some researchers proposed environmentally benign approaches by using organic acids or green solvents, these approaches still face their own set of challenges. For example, the leaching speed with oxalic acid is low, and it is unable to fully dissolve the cathode active materials, restricting its large-scale application (*22*). In contrast, the deep eutectic solvent can act as both a leaching and reducing agent for $LiCoO_2$ and $LiNi_{1/3}Mn_{1/3}Co_{1/3}O_2$ battery recycling, but its lithium recycling efficiency is limited and not suitable for the $LiFePO_4$ (LFP) batteries (*23*). The biometallurgy

[1]Research Center of Grid Energy Storage and Battery Application, School of Electrical Engineering, Zhengzhou University, Zhengzhou 450001, China. [2]State Key Laboratory of Alternate Electrical Power System with Renewable Energy Sources, School of New Energy, North China Electric Power University, Beijing 102206, China. [3]Key Laboratory of Power Station Energy Transfer Conversion and Systems, Ministry of Education, North China Electric Power University, Beijing 102206, China. [4]Centre for Clean Energy Technology, School of Mathematical and Physical Sciences, Faculty of Science, University of Technology Sydney, NSW 2007, Australia. [5]Centre for Cooperative Research on Alternative Energies (CIC energiGUNE), Basque Research and Technology Alliance (BRTA), Alava Technology Park, Albert Einstein 48, 01510 Vitoria-Gasteiz, Spain. [6]State Key Lab of New Ceramics and Fine Processing, School of Materials Science and Engineering, Tsinghua University, Beijing 100084, China.
*Corresponding author. Email: yangjin@zzu.edu.cn (Y.J.); liukai21@ncepu.edu.cn (K.L.); huiwu@tsinghua.edu.cn (H.W.); marmand@cicenergigune.com (M.A.); guoxiu.wang@uts.edu.au (G.W.)

method uses biodegradable materials to extract Li source materials from the spent LIBs. Although this approach is economical, it requires a long treatment period using incubating microbes and acids (*24*). In addition, electrochemical extraction methods that separate lithium from the pretreated active materials by using a lithium-selective membrane have been reported. For instance, lithium aluminum titanium phosphate (LATP) solid membrane (19 mm in diameter and 800 μm in thickness) has been applied in the lithium extraction at a laboratory scale (*25*), but the reaction processes were complex and the bath voltage was high, which raises the overall cost for the system construction. Hence, there is an urgent need for a sustainable and green lithium recovery technique for spent LIBs (*26*). Through this strategy, it should be possible to economically achieve high lithium recovery efficiency without disturbing the other valuable metal recycling.

Recently, $Li_7La_3Zr_2O_{12}$ (LLZTO)–based Li-stuffed garnet-type solid electrolyte materials have attracted wide attention in the field of solid-state lithium batteries (*27*–*29*). The LLZTO-based solid electrolyte materials have many physical and chemical advantages including (i) high Li^+ conductivity (10^{-4} to 10^{-3} S cm^{-1}) at room temperature (*30*); (ii) excellent chemical stability with elemental Li (*31*); and (iii) wide electrochemical window (up to 5 V versus Li^+/Li) (*32*). It has superior selectivity for Li^+ conduction and can simultaneously block other interfering cations in aqueous solutions. Therefore, the LLZTO-based solid electrolyte materials have promising potential to work as a medium to selectively extract lithium ions from the spent LIBs. Nevertheless, the applications of LLZTO for lithium recycling of spent LIBs have not been reported.

Notably, the stability of LLZTO in aqueous solutions directly affects the lithium recovery efficiency of spent LIBs. Spontaneous Li^+/H^+ ion exchange has been reported for LLZTO in aqueous solutions such as LiOH, LiCl, and deionized (DI) water (*33*, *34*). Such reactions between Li^+ in LLZTO and H^+ in aqueous solutions do not change the cubic garnet structure of LLZTO but diminish the Li^+ transport (*34*, *35*). To restore H_2O-poisoned LLZTO (H-LLZTO) to its original stoichiometry, most studies focus on compensating lithium sources by deprotonating and decomposing impurities at high temperatures (*36*). Nevertheless, complete decomposition of Li_2CO_3 usually requires ~1000°C treatment (*37*). Meanwhile, the volatilization of Li_2O at such high temperature will inevitably cause the formation of $La_2Zr_2O_7$ (LZO), which has low ionic conductivity (2.64×10^{-7} S cm^{-2}) and will seriously hinder the migration of Li^+ ions (*38*, *39*). Therefore, it is critical to modify the surface of pristine LLZTO to be hydrophobic using ionically conducting waterproof materials. This is required to inhibit the proton exchange with water molecules, but without affecting the transport of Li^+ ions in the LLZTO during the recycling process.

In this work, we aim to achieve high-purity lithium recycling from spent LIBs. We report a green and nondestructive lithium recycling strategy of spent LIBs based on the bis((trifluoromethyl) sulfonyl)azanide and poly(3-hexylthiophene-2,5-diyl) (denoted as LiTFSI+P3HT)–modified LLZTO solid electrolyte. This system can realize the high-purity enrichment of lithium in the form of LiOH, while blocking interfering ions at an affordable cost without causing contamination. This lithium recycling strategy also involves the production of H_2 gas, which could be collected for green energy utilization and partially compensate the total energy cost of the recycling processes. The P3HT modification of the LLZTO surfaces enables LLZTO to be compatible with aqueous solutions. In general, the LiTFSI+P3HT-modified LLZTO realizes roll-to-roll lithium extraction, which is different from the existing recycling method for spent batteries. This new process does not require pretreatment of spent batteries that involves separating cathode materials from their Al foil substrates and organic binders. Therefore, our new technique will endow better lithium recovery efficiency without causing any loss of other valuable metal in spent batteries. Compared with previous work (*40*); from another perspective, we proposed a new strategy to turn "waste" into the wealth without consuming the natural lithium reserves.

RESULTS

Design of lithium recycling system for spent LIBs

We designed a roll-to-roll lithium recycling system for spent LIBs as shown in Fig. 1. The detail information about each part of the lithium recycling device is presented in fig. S1. The key component of this system is the solid ceramic lithium-ion electrolyte tube. By comparing the lithium-ion conductivity, density, and stability at room temperature of various solid-state electrolyte materials, we selected the garnet-type $Li_{6.4}La_3Zr_{1.4}Ta_{0.6}O_{12}$ (LLZTO) ceramic to fabricate solid electrolyte tubes in this work. The operating temperature of this system is set to 50°C to maintain high Li^+ conductivity of the LLZTO. The lithium recycling process was conducted in a drying box filled with N_2 atmosphere.

By charging the system, Li^+ ions from the Li-containing electrode (anode compartment) wetted by the electrolyte move to the cathode compartment and form LiOH. In detail, the hydrolysis of water in the cathode compartment leads to the formation of OH^- and H^+ ions. The OH^- ions react with the extracted Li^+, forming LiOH. Simultaneously, H^+ ions acquire electrons from the external circuit, resulting in the generation of H_2 gas. Thereby, this process drives the transport of Li^+ from the Li-containing electrode through the selectivity of LLZTO@P3HT and then is enriched in the cathode compartment. Figure 1 illustrates the overall reactions and working principle of the lithium extraction process, and the details about the H_2 gas capture design for further green energy utilization is provided in fig. S2. A demonstration video about this roll-to-roll lithium recycling process of $LiFePO_4$ (LFP) electrode is provided in movie S1. It is clear to see that this roll-to-roll setup can achieve double-side and repeatable recycling of the lithium-containing electrode without destroying its integrity. Because the intact structure of the electrode is preserved by this technique, it can also be used for other valuable metal recycling.

Waterproof protection of LLZTO

According to a previous report (*33*), bare LLZTO experiences a rapid and spontaneous Li^+/H^+ exchange with water molecules after exposure to aqueous solutions such as LiOH, LiCl, and DI water. As shown in Fig. 2A, the Li^+ concentration of a solution of LiOH, LiCl, and DI water grows appreciably with the immersion time when in contact with bare LLZTO. Although the cubic structure of bare LLZTO persists after proton exchange in the aqueous environment (fig. S3), it still suffers from degradation in the Li^+ conductivity (fig. S4) due to the following: (i) the formation of side products on the bare LLZTO surfaces and (ii) the slowing of ion hopping in the ceramic bulk due to the presence of H^+ sites. Obviously, bare LLZTO is unstable in the water environment, which will affect its long-term service and degrade the lithium extraction performances. Thereof, it is necessary to improve the stability of LLZTO in the aqueous solutions.

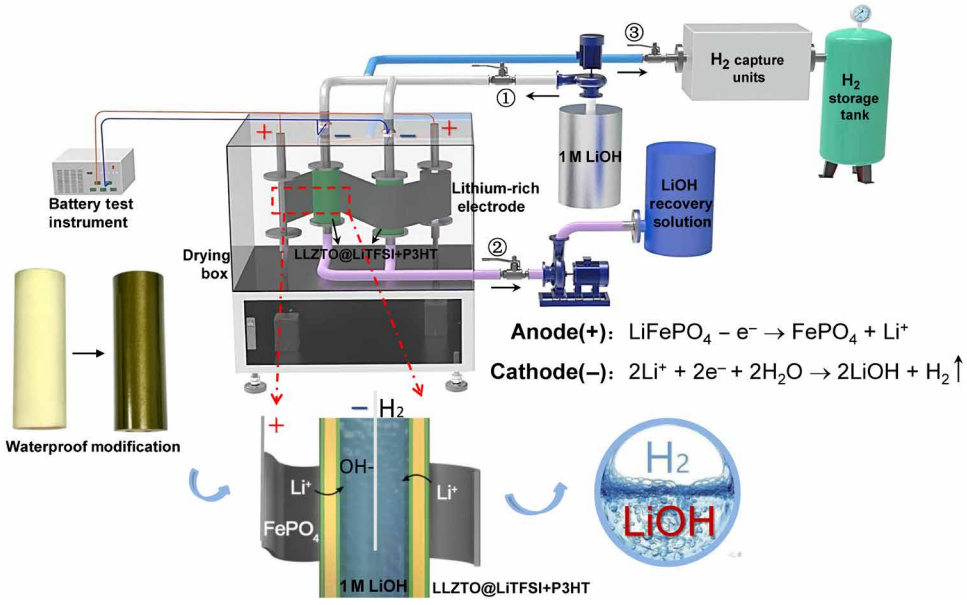

Fig. 1. Schematic procedure for a green and nondestructive lithium resource recycling system for spent LIBs. The working principle of this system relies on the current driven Li^+ diffusion through a high-selectivity LLZTO tube.

To solve the problem of Li^+ dissolution from the LLZTO in the aqueous solutions, we conducted surface coating on the outer and inner surfaces of a bare LLZTO tube. The surface coating layer is required to have excellent water stability and to conduct lithium ions at the working temperature of lithium recycling, so as to not affect the conduction and enrichment of Li^+ through the LLZTO tube. As we all know, the proper combination of polymer and lithium salts can form a Li^+ polymer electrolyte system, which has good Li^+ conductivity at room temperature. On the basis of this condition, we adopted P3HT+LiTFSI as the composition of an LLZTO coating layer, where P3HT works as the waterproof material and LiTFSI ensures the Li^+ conductivity of the coating layer.

First, to prove the waterproof ability of P3HT, we prepared a pure P3HT film as shown in Fig. 2B. The thickness of the as-prepared film can be well controlled on the basis of the amount of the polymer solution applied. Notably, once immersed into water, the pure P3HT film floats on the surface without being wetted (fig. S5). Figure 2C and fig. S6 show the dynamic water contact angle of pure P3HT film to be 108.5°, demonstrating its hydrophobic nature. Moreover, the pure P3HT film can remain freestanding and structurally stable for a relatively long period of time (6 months) without additional treatment (fig. S7). Thermogravimetric analysis of P3HT demonstrates its stability in the working temperature (50°C) of lithium recycling system as it begins to thermally degrade at 420°C (fig. S8).

Second, to further prove that the LiTFSI+P3HT coating layer can realize waterproof and Li^+ conduction, we designed the experiments in the H-type container as shown in Fig. 2D; the LiTFSI+P3HT film was placed in the middle of an H-type container to separate different amounts of water on each side. At the beginning, we added a drop of red ink into the left side, which has the highest liquid level; after 12 hours, neither color changes nor an increase in the liquid level was observed on the right side of the container, showing that the LiTFSI+P3HT film has perfect compact structure without any porosity to allow water penetration. On the basis of this excellent compactness, we then respectively used a rubber mat, a P3HT+LiTFSI film, and no separator to part equal amounts of LiOH solution on each side of the H-type cell; Pt electrodes were used as the cathode and anode current collectors. The electrochemical impedance spectroscopy (EIS) was provided in Fig. 2E. Because the rubber mat is an ionic insulator, lithium ions cannot diffuse through it in the LiOH solution, so its EIS spectrum is erratic and at high Z values (fig. S9). While the LiTFSI+P3HT film exhibits the typical property of ion-conducting polymers, we see a single semicircle at high frequencies and a capacitive tail at low frequencies in the EIS. The detailed parameter identification was provided in fig. S10 and table S1. Thereof, the above analysis identifies the waterproof and Li^+ conduction features of the prepared LiTFSI+P3HT film.

Figure 2F shows the cross-sectional view of the LLZTO tube after LiTFSI+P3HT coating; we can observe that the coating layer is around 5 μm in thickness with evenly distributed C and S elements (Fig. 2G). Compared with the hydrophilic nature of bare LLZTO (water contact angle, 26.9°), the LiTFSI+P3HT- modified LLZTO surface exhibits hydrophobicity property with the dynamic water contact angle of 106.5° (fig. S11). To examine the waterproof effectiveness of LiTFSI+P3HT coating layer on the LLZTO surface, we soaked bare LLZTO and LLZTO@LiTFSI+P3HT ceramic electrolyte tubes in DI water, 1 M LiOH solution, and saturated LiCl solution, respectively, and then sealed them to reduce water evaporation loss. Samples (1 ml) were taken out every 7 days, and the Li^+ concentration was measured by inductively coupled plasma optical emission spectrometry (ICP-OES) as illustrated in Fig. 2A. Although LiCl and LiOH solution slightly reduce the H^+/Li^+ ion exchange with bare LLZTO, the Li^+ dissolutions are still slowly progressing and reaches 150 ppm within 30 days. In contrast, as for the LLZTO@LiTFSI+P3HT tube, whatever it is soaked in (1 M LiOH solution, saturated LiCl and DI water for 1 month), the Li^+ concentration remained stable and the value change is less than 15 ppm. This identifies that the LiTFSI+P3HT coating layer effectively protects the LLZTO from water corrosion. Therefore, water molecules cannot penetrate

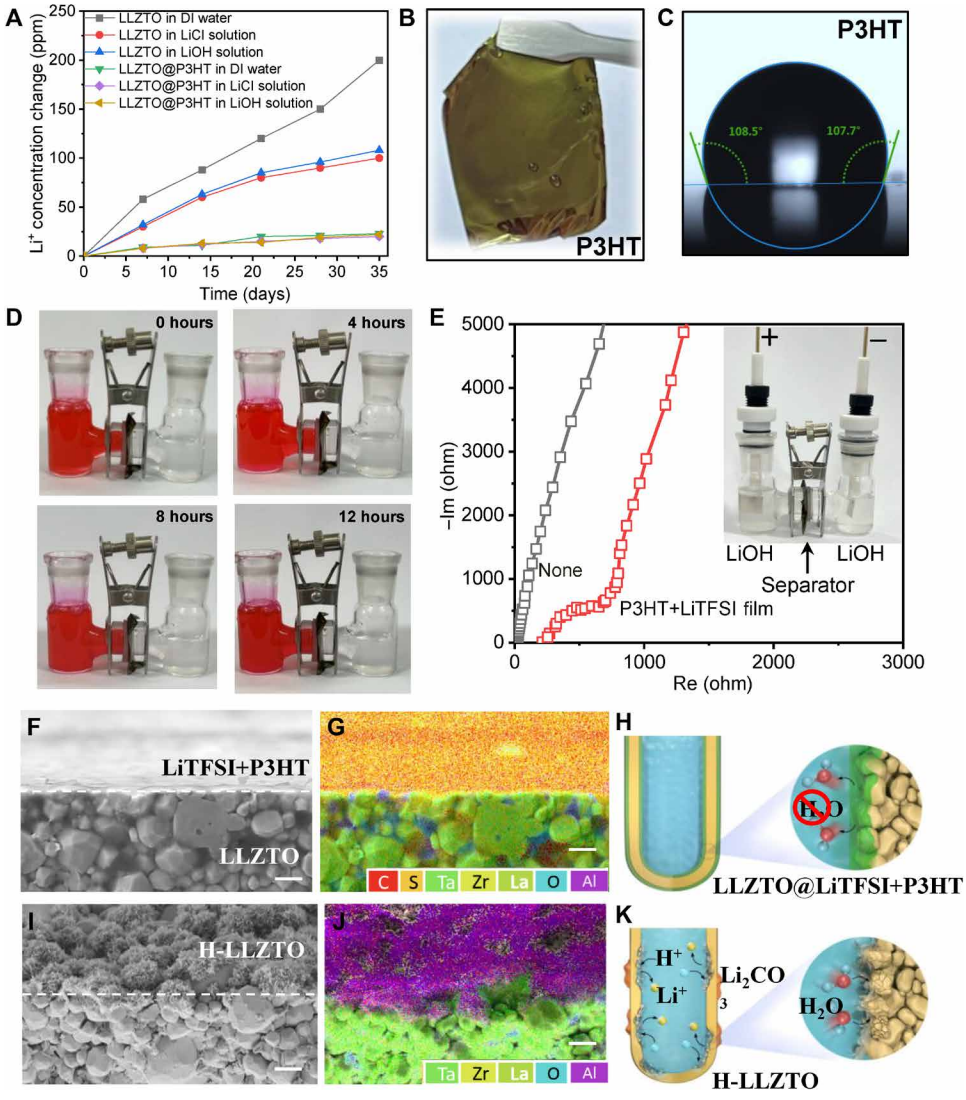

Fig. 2. Physical characterizations of P3HT+LiTFSI-modified LLZTO. (**A**) Li^+ concentration changes of different solutions after immersion of LLZTO, LLZTO@P3HT+LiTFSI and DI water. (**B**) Pure P3HT film. (**C**) Dynamic water contact angle of pure P3HT film. (**D**) Compactness evaluation of P3HT+LiTFSI film. (**E**) EIS of the H-type cell based on the different separators (the effective test area of each separator is fixed with diameter of 12 mm). (**F**) Scanning electron microscopy (SEM) image and (**G**) the corresponding EDS of LiTFSI+P3HT-modified LLZTO. Scale bars, 10 μm. (**H**) Schematic illustrating the waterproof nature of LLZTO@LiTFSI+P3HT. (**I**) SEM image and (**J**) the corresponding EDS of bare LLZTO after immersion in water for 2 weeks. Scale bars, 10 μm. (**K**) Schematic illustrating the H^+/Li^+ ion exchange between bare LLZTO and H_2O.

into the bulk garnet LLZTO and Li^+ diffusion from LLZTO can be notably suppressed. Moreover, fig. S12 presents digital photos of the LLZTO@LiTFSI+P3HT tube after immersion in 1 M LiOH solution for 2 months. We can see that the LiTFSI+P3HT layer closely adheres to the LLZTO tube, and no notable surface changes were observed. On the other hand, given that 1.2 wt % Al_2O_3 was added to the synthesis precursors of LLZTO, the grain boundary of LLZTO contains $LiAlO_2$ phase which is unstable in water (*34*), the impurity $Al(OH)_3$ often formed on the bare LLZTO when exposed to water (Fig. 2, I and J, and figs. S13 and S14), impeding Li^+ transport across the grain boundaries. Now, after P3HT modification, the impurity $Al(OH)_3$ with flake morphology does not appear in the LLZTO@LiTFSI+P3HT tubes immersed in 1 M LiOH solution for 1 month (fig. S15). Because LiOH is formed on the cathode of our lithium recycling system, the above alkaline condition is closer to the practical application, indicating that the LiTFSI+P3HT-modified LLZTO tubes are stable in the lithium recycling environment.

Properties of P3HT on LLZTO surface based on density functional theory calculations

To investigate the interaction between P3HT and water, we dissolve single P3HT unit in water molecules, as shown in Fig. 3A, in which a clear boundary between a hydrophobic alkyl group and the surrounding water has been observed and shown with a dashed green line. Following this result, it is reasonable to expect that P3HT-protected surface may present hydrophobic feature and thus offers excellent stability in an aqueous environment. The computational

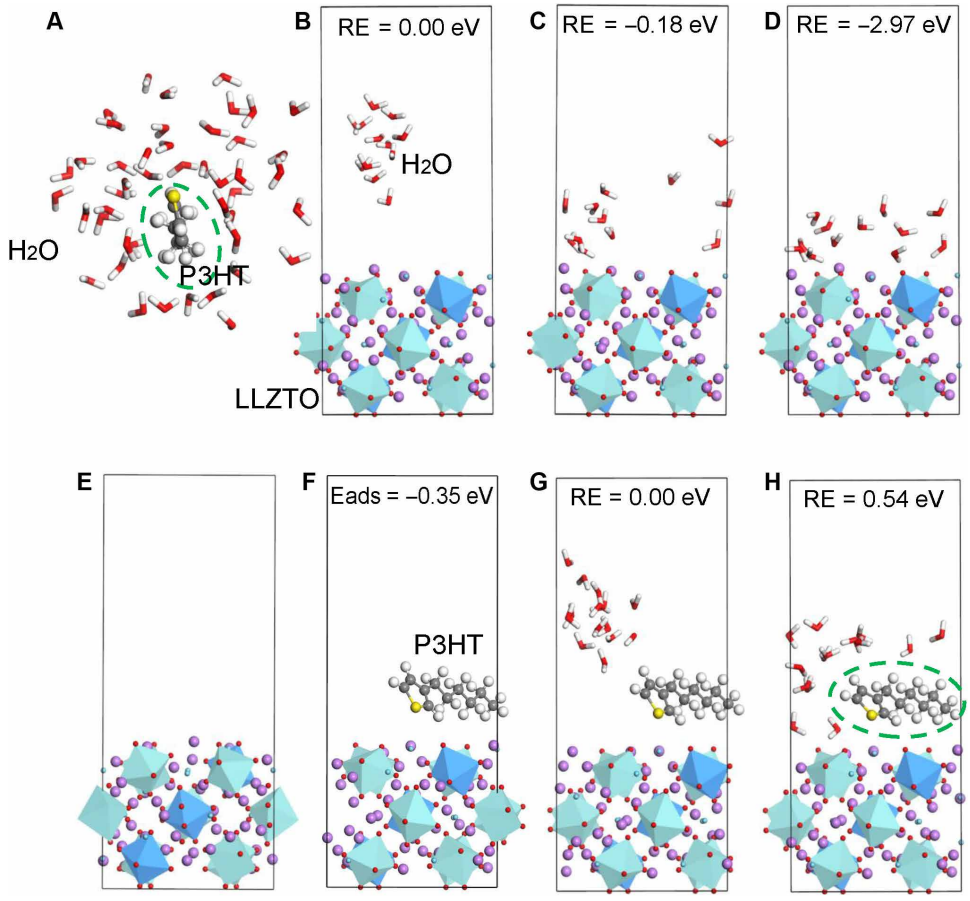

Fig. 3. Protection mechanism of P3HT on the LLZTO surface. (**A**) Geometry of P3HT dissolved in water. The green circle shows a notable gap between P3HT (ball-and-stick) and water molecules (stick). (**B** to **D**) Density functional theory (DFT) calculation of water adsorption on bare LLZTO surface. (B) Water cluster being away from the surface, serving as a reference state with relative energy (RE) = 0.00 eV. (C) Partially adsorbed water with RE = −0.18 eV. (D) Stable water layer on the surface with RE = −2.97 eV. (**E**) Bare LLZTO (010) surface. (**F** to **H**) DFT calculation of water adsorption on P3HT-protected LLZTO surface. (F) P3HT adsorption. (G) Water cluster being away from P3HT-adsorbed surface, serving as a reference with RE = 0.00 eV. (H) Water adsorbed around P3HT and LLZTO surface with RE = 0.54 eV. Li, La, and O are shown as purple, aquamarine, and red balls, respectively; H_2O as stick; and ZrO_6 and TaO_6 units as aquamarine and blue polyhedrons, respectively.

model of LLZTO bulk and (010) surface is provided in fig. S16. To investigate water adsorption, we introduce 12 water molecules to the LLZTO (010) surface. Given that water-water hydrogen bonding plays a key role, our investigation starts with a water cluster away from the surface as the reference [Fig. 3B, relative energy (RE) = 0 eV]. When water molecules get close to the LLZTO (010) surface, some prefer to adsorb as shown in Fig. 3C, showing slightly lower energy (RE = −0.18 eV). When more molecules reach the surface (Fig. 3D), a stable water layer is generated as determined by water-water hydrogen bonds and water/LLZTO interfacial interaction. Such adsorption is energetically favorable, as highlighted by the large RE = −2.97 eV, which clearly identifies strong water adsorption on bare LLZTO surface.

Second and more importantly, we turn to the discussion of P3HT adsorption and its protection for LLZTO surface. Starting with a bare LLZTO (010) surface as shown in Fig. 3E, a single P3HT unit has been introduced and stable adsorption geometry has been achieved as presented in Fig. 3F, which shows typical physical adsorption with an adsorption energy E_{ads} = −0.35 eV, with polarized sulfur termination pointing to Li/La sites. Over such P3HT-preadsorbed surface, water cluster $(H_2O)_{12}$ has been introduced as shown in Fig. 3G; however, further adsorption to the surface (Fig. 3H) is not energetically favorable. Specifically, an energy increment of 0.54 eV resulted when the geometry changes from that in Fig. 3G to that in Fig. 3H, which is remarkably different from water adsorption on bare LLZTO (010) surface, as demonstrated in Fig. 3D. This is not unexpected because pre-adsorbed P3HT is dominated by a hydrophobic alkyl group, which protects the surface from water adsorption. As vividly demonstrated in Fig. 3H, a clear boundary between P3HT and water molecules has been observed, as labeled by the dashed green line. Overall, pre-adsorbed P3HT can protect LLZTO surface from water adsorption due to the repulsion between the hydrophobic alkyl group and water.

Lithium recycling performance for spent $LiFePO_4$ batteries

Beyond fundamental studies in the working principle of our roll-to-roll lithium recycling system, we envision this concept to be applicable to the selective recovery of lithium from spent LIBs, providing a sustainable pathway for lithium recycling of spent LIBs. To provide a proof of feasibility, we pretreated commercial 18650 1.2 Ah $LiFePO_4$ battery through discharging, dismantling, and then undergoing the roll-to-roll lithium recycling processes as shown in Fig. 4A. For the

details of the lithium recycling process, an 8.0 g $LiFePO_4$ electrode that includes 7.11 g $LiFePO_4$ materials (Q_{actual} = 155 mAh/g) and 0.89 g Al foils were loaded on the anode compartment, and LiTFSI+P3HT-treated LLZTO tubes filled with 1 M LiOH solution work as the cathode part of the roll-to-roll setup. For comparison, the bare LLZTO–based roll-to-roll setup was prepared with the same conditions. Both of setups were charged at a current of 1 mA/cm^2 until the voltage increased to 3.5 V. During the lithium recycling process, the H_2 gas was continuously detected by gas chromatography (Fig. 4B). Specifically, when 1 mol of Li^+ ions is extracted, 0.5 mol of H_2 gas (corresponding to about 11.2 liters of H_2 gas at T = 273.15 K and P = 101.325 kPa) will be produced, the produced H_2 can be collected for green-energy utilization. In addition, the x-ray diffraction (XRD) pattern of the LFP electrodes in both groups after lithium extraction exhibits $FePO_4$ phase (PDF#34-0134), confirming the successful extraction of lithium from the pristine $LiFePO_4$ electrode under the imposed current (Fig. 4C). Moreover, time-of-flight secondary ion mass spectrometry (TOF-SIMS) was also performed to visually illustrate

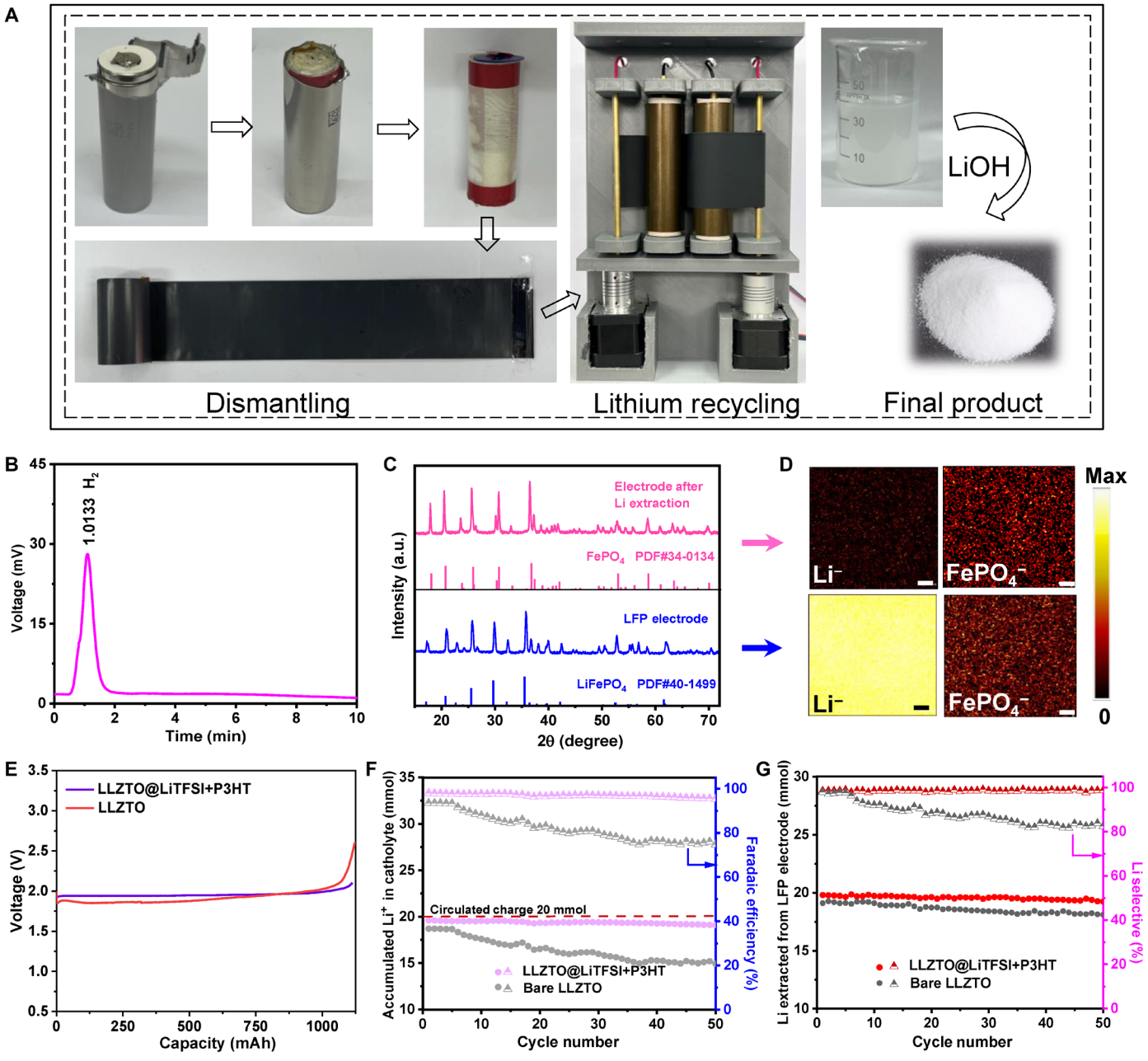

Fig. 4. Application of the roll-to-roll system for potential use in lithium recycling of spent $LiFePO_4$ battery. (**A**) Lithium extraction processes for spent $LiFePO_4$ battery based on the P3HT-treated LLZTO recycling systems. (**B**) H_2 gas was captured during the Li extraction process through the automatic gas chromatography detection. (**C**) XRD patterns of the $LiFePO_4$ electrode before and after Li extraction. (**D**) TOF-SIMS of the $LiFePO_4$ electrode before and after Li extraction. Scale bars, 1 μm. (**E**) The Li extraction profiles for the untreated and P3HT-treated LLZTO based roll-to-roll setups under the current driven. (**F**) ICP-OES measured Li increasement in the LiOH catholyte and the corresponding Faradaic efficiency during cycles. (**G**) ICP-OES measured Li extraction amount from the $LiFePO_4$ electrode and the corresponding Li selectivity during cycles.

the lithium content and elemental distributions in the LFP electrodes (Fig. 4D). The TOF-SIMS spectra were collected over time from the ejected secondary ions sputtered by Ar ions. After sputtering, a relatively uniform distribution of secondary ions of Li^- and $FePO_4^-$ species was observed on the surface of the pristine LFP electrode, while for the LFP electrode after Li extraction, the signal of Li^- species is almost absent and $FePO_4^-$ species remains unchanged. These results visually elucidated that lithium has been extracted from the $LiFePO_4$ electrode by using our lithium recycling device. The corresponding lithium extraction profiles for the untreated/P3HT-treated LLZTO–based setups are presented in Fig. 4E, in which the circulated charge capacity recorded by the battery test machine were 1113 and 1124 mAh, respectively. Then, ICP-OES was applied to characterize the elemental changes in the catholyte and the LFP electrode before and after Li extraction. After lithium extraction, no Fe element in the LFP electrode was detected in both catholytes (figs. S17 and S18). Meanwhile, the Li element in both LFP electrodes decreased from 42.72 to 0 mmol, while the Li element in catholytes increased from 70 to 111.83 mmol and 110.75 mmol for the LLZTO@LiTFSI+P3HT and bare LLZTO tubes, respectively. This result verifies that LLZTO ceramic electrolyte has a unique selectivity for Li^+ while blocking the migration of other interfering ions. In addition, the circulated charge recorded by the battery test machine is calculated to be around 43.03 and 44.26 mmol for the LLZTO@LiTFSI+P3HT- and P3HT-based setups, respectively. Thus, the Faradaic efficiency determined by the ratio of Li increase (mmol) in the catholyte to the circulated charge was 97.19% (LLZTO@LiTFSI+P3HT) and 92.05% (LLZTO). Meanwhile, the Li selectivity evaluated as the ratio between the Li increase (mmol) in the catholyte and the Li extraction from the LFP electrode was 97.92% (LLZTO@LiTFSI+P3HT) and 95.41% (LLZTO). Therefore, it is clear that the Li selectivity for the untreated and P3HT-treated LLZTO tubes do not show substantial differences in their initial state, and the small gap (5.14%) in the Faradaic efficiency is ascribed to the side reaction of bare LLZTO in the aqueous solution, which causes extra consumption of electrical energy.

Furthermore, to better evaluate the performances of the untreated and P3HT-treated LLZTO in the roll-to-roll setups, especially in terms of the long-term stability, selectivity, and electric energy consumption, we conducted cycling performance tests. Both the untreated and P3HT-treated LLZTO tubes were filled with 1 M LiOH solution as the started catholyte and the fresh LFP electrode with 800 mAh actual capacity as the anode. This time, the lithium extraction processes were conducted at a constant current of 1 mA/cm^2 until the accumulated charge capacity reaches 500 mAh (equal to 20 mmol accumulated charge), and then the recycling stops and the LFP electrode and the catholyte are changed to the fresh condition. This procedure is repeated 50 times to obtain 50 samples of LFP electrode and catholyte after lithium extraction, numbered from 1 to 50 in sequence. The cycling performance of the untreated and P3HT-treated LLZTO are provided in Fig. 4, F and G. We can see that the P3HT-treated LLZTO roll-to-roll setup shows excellent stability in both the Li increment in the catholyte and the Li extraction from the LFP electrode. After 50 cycles, its Faradaic efficiency that represents the utilization rate of electric energy remains at 97.12%, and the Li selectivity is stable at 98.11%. In contrast, the performance at the start of the bare LLZTO–based recycling system is satisfactory, but because of the lithium dissolution from bare LLZTO in the LiOH catholyte and other side reactions, it shows serious degradation in the Faradaic efficiency and the Li selectivity beyond cycle 10. Therefore, from the perspectives of long-term stability, selectivity, and electrical energy utilization, the P3HT-treated LLZTO exhibits excellent Li recovery performances based on our roll-to-roll setup.

The inset of Fig. 4A illustrates the enrichment of the LiOH solution after lithium extraction from the LFP electrode. White powder was obtained by evaporating the concentrated LiOH solution after the recycling was completed. The collected white powder was characterized by XRD (fig. S19), whereby the XRD pattern fits well with the standard pattern of anhydrous LiOH (PDF#32-0564) without any impurity signals being detected. Further quantitative elemental analyses show that the purity of LiOH was 99.94 ± 0.03%, and the weight percentages of Fe, La, Zr, and Ta in the product were 0.93 ± 0.03, 0.99 ± 0.02, 2.16 ± 0.02, and 3.18 ± 0.01 ppm, respectively. All the above results reveal that our roll-to-roll lithium extraction setup with the configuration of "lithium-rich electrode (anode)||LLZTO@P3HT||LiOH" is feasible, and the enriched LiOH solution obtained is pure enough to be applied for further industrial processing.

However, in practice, this system seems could not operate only on the condition that the liquid electrolyte is sufficiently buried in the waste electrode. Sometimes, the waste Li-containing electrodes usually already dry when dismantled from the spent batteries. To solve these difficulties caused by the contact resistance, we separated the dry LFP electrode from the spent battery and wetted it with DI water in the air atmosphere and then conducted the lithium extraction test in the air based on our system. The corresponding lithium extraction profile for waste LFP battery is shown in fig. S20, and we can see that our system can still work in the air even when the disassembled electrode was dry. As for reasons, there are still plenty of lithium salt attached on the surface of the dry electrode; when wetting its surface with DI water, this lithium salt dissolves in the DI water and helps the Li^+ transfer. To prove that the working principle of our work is feasible, we previously conducted the lithium extraction tests and characterizations in the drying box with N_2 atmosphere, which helps to avoid all the possible disturbances in the air. In this part, we further consider the practical condition; instead of applying organic electrolyte, we used DI water to wet the electrode and conducted the lithium extraction processes in the air, which proves to be feasible and confirms the practicability of our lithium extraction system.

Lithium recycling performance for spent $LiNi_{0.5}Co_{0.2}Mn_{0.3}O_2$ batteries

To confirm the universal application of our lithium recycling system, we further evaluate the lithium recycling performance for the spent $LiNi_{0.5}Co_{0.2}Mn_{0.3}O_2$ (NCM523) battery with the actual specific capacity of 554 mAh/g. As shown in Fig. 5A, $Li_{0.06}Ni_{0.5}Co_{0.2}Mn_{0.3}O_2$ phase (PDF#85-1977) was obtained after lithium extraction, which can be further identified by the x-ray photoelectron spectroscopy (XPS) results (fig. S21). This XRD result also corroborates the electrochemical Li extraction behaviors of NCM523 electrode as shown in Fig. 5B. Meanwhile, the element intensity variations in the NCM523 electrode before and after lithium extraction were detected by TOF-SIMS (Fig. 5, C and D and fig. S22). The signals of Ni^-, Co^-, and Mn^- in the electrode after lithium extraction remain almost unchanged in the three-dimensional imaging (Fig. 5C) and depth profiles of the TOF-SIMS (Fig. 5D). In contrast, the signal of Li^- diminishes

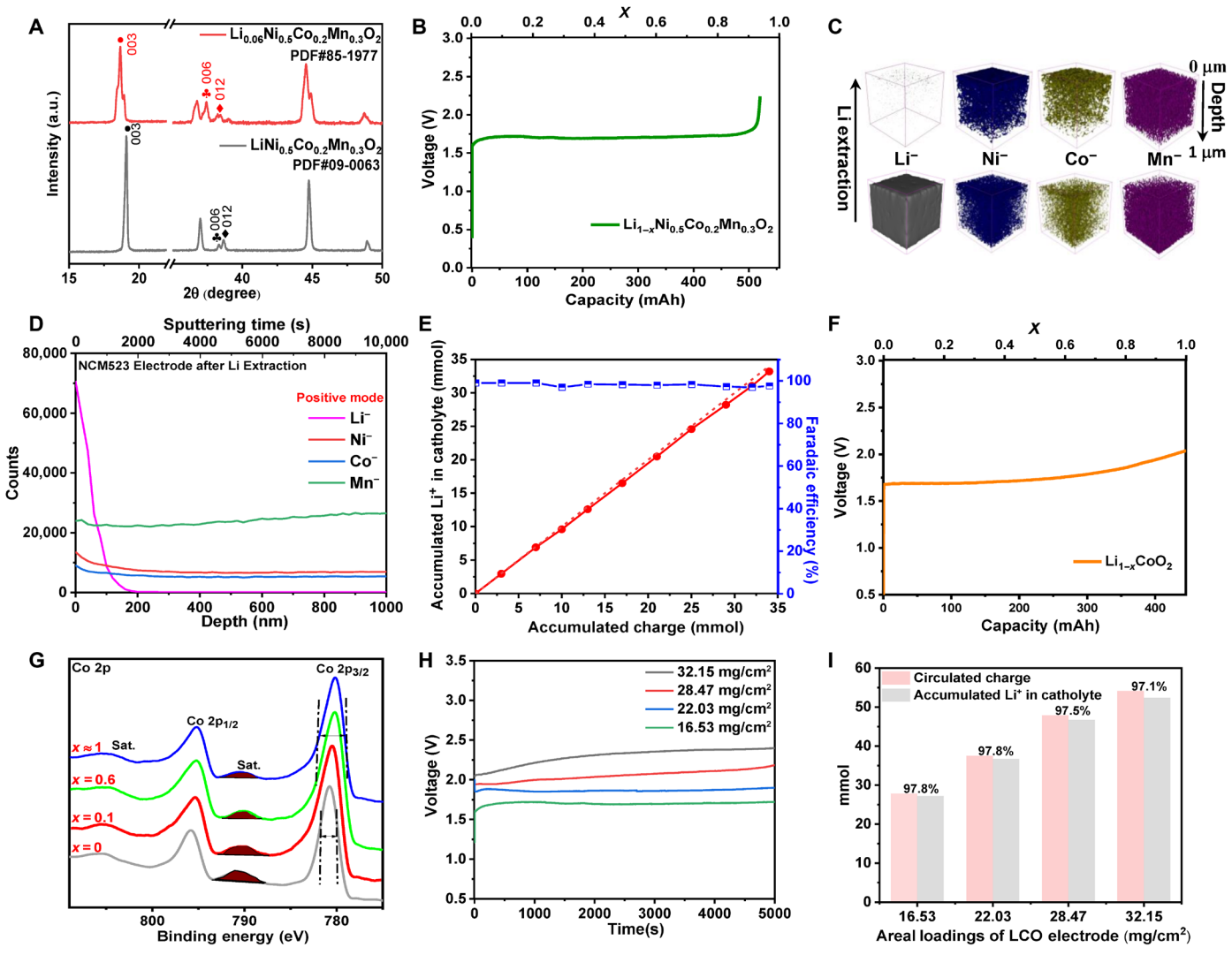

Fig. 5. Characterizations and electrochemical performance of lithium recycling from spent $LiNi_{0.5}Co_{0.2}Mn_{0.3}O_2$ and $LiCoO_2$ batteries. (**A**) XRD patterns of the $LiNi_{0.5}Co_{0.2}Mn_{0.3}O_2$ electrode before and after Li extraction. (**B**) The Li extraction profiles of $LiNi_{0.5}Co_{0.2}Mn_{0.3}O_2$ electrode under current driven. (**C**) TOF-SIMS three-dimensional images of an $LiNi_{0.5}Co_{0.2}Mn_{0.3}O_2$ electrode before and after lithium extraction. (**D**) TOF-SIMS depth profile of $LiNi_{0.5}Co_{0.2}Mn_{0.3}O_2$ electrode before and after lithium extraction. (**E**) ICP-OES measured Li increasement in the LiOH catholyte and the corresponding Faradaic efficiency during $LiNi_{0.5}Co_{0.2}Mn_{0.3}O_2$ electrode recovery. (**F**) The Li extraction profiles of an $LiCoO_2$ electrode under current driven. (**G**) Co 2p XPS core peaks of $Li_{1-x}CoO_2$ ($0<x<1$) electrode during lithium extraction. (**H**) The voltage-time profiles for the lithium extraction of $LiCoO_2$ electrodes with the surface mass densities of 16.53, 22.03, 28.47, and 32.15 mg/cm^2. (**I**) The Faradaic efficiency for $LiCoO_2$ electrodes with different areal loadings.

with depth, demonstrating that the lithium extraction from the NCM523 electrode is uniform and homogeneous. Furthermore, during different lithium extraction stages, the corresponding Faradaic efficiency determined by the ratio of transmembrane Li^+ flux (mmol) to the circulated charge was provided in Fig. 5E. The former was obtained by measuring the Li^+ increment in catholyte, for which the catholyte was taken from the LLZTO@P3HT tube for ICP-OES measurement. The stepwise increase in the circulated charge nearly equals the amount of Li^+ accumulation in the catholyte across the LLZTO@P3HT tubes, and the overall Faradaic efficiency is above 98.2%. Such a high Faradaic efficiency is ascribed to the negligible side reactions. As a result, the catholyte in essence consists of pure LiOH solution, whose concentration increases with time upon continuous operation.

Lithium recycling performance for spent $LiCoO_2$ batteries

To further prove the feasibility of the lithium recycling system, we extended it to the $LiCoO_2$ (LCO) electrode with the actual capacity of 450 mAh. The corresponding recycling profile is shown in Fig. 5F. For the delithiated $Li_{1-x}CoO_2$ electrode, there is no clear difference in XRD patterns compared with the pristine $LiCoO_2$ electrodes (fig. S23). A slight shift of the (003) plane to lower 2θ angles is noticeable in the delithiated electrode because of a lower Li/Co atomic ratio (*41*). Figure 5G shows the Co 2p XPS core peaks of the $Li_{1-x}CoO_2$ electrode during lithium recycling. To our knowledge, the precise energy position and the relative intensity of the satellite characteristics of Co^{4+} ions in an oxygen environment have not been reported previously. However, when Li^+ was deintercalated from $LiCoO_2$, the full width at half-maximum of the Co 2p3/2 main

peak increased from 1.8 to 3.1 eV, and the relative satellite peak area decreases from 9.0 to 4.6% (table S2). Similarly, as shown in the Co 3p XPS core peaks of the same samples (fig. S24), we observed a strong broadening of the main peak toward higher binding energies upon lithium extraction. All these observations are consistent with previous reports, which can be attributed to the oxidation process of Co^{3+} (*42*). These XPS results are consistent with the electrochemical Li extraction behavior of the LCO electrode.

Given that high areal loading of the electrode is crucial to the energy density of batteries in practical application, we further evaluated the lithium recycling performance of the LCO electrodes (300 mm in length × 55 mm in width) with different areal loadings (16.53, 22.03, 28.47, and 32.15 mg/cm^2) based on the P3HT-treated roll-to-roll setup. As shown in Fig. 5H, the voltage-time profiles for the LCO electrode with the areal loading of 16.53, 22.03, 28.47, and 32.15 mg/cm^2 show the charge potentials of 1.69, 1.85, 2.02, and 2.33 V, respectively. Among these four sets, we calculated the Faradaic efficiency determined by the ratio of Li^+ increment in catholyte (mmol) to the circulated charge as shown in Fig. 5I. Notable variations do not show up in the Faradaic efficiencies for these LCO electrodes with different areal loadings. Even with the areal loading of 32.15 mg/cm^2, the Faradaic efficiency of 97.1% can still be achieved, demonstrating that our roll-to-roll recycling system is feasible for electrodes with high active material loading.

Economic evaluation for our lithium recycling strategy

As acknowledged, a sustainable recycling method is generally characterized by minimal water and electricity usage, as well as prevention of the release of polluting gases and waste residues to the environment. However, beyond this, the economic assessment is also necessary to guarantee the sustainability of such recycling methods. If the income is lower than the recycling cost, then recycling would not be economically appropriate or viable. Thereof, we carried out a technoeconomic analysis by considering the market prices of the reagents, products, and energy consumptions involved in the lithium recycling process of spent batteries. For example, the lithium recycling process from the spent $LiFePO_4$ batteries was divided into three parts including the separation of $LiFePO_4$ electrode, lithium extraction process (LiOH enrichment), and the regeneration of Li in the form of Li_2CO_3. As shown in Fig. 6 and note S1, taking the recycling of 1.0 kg of spent $LiFePO_4$ batteries as an example, the input costs are composed of the raw materials for spent $LiFePO_4$ batteries ($1.0) and LLZTO@P3HT membrane ($1.41), the initial anode solution ($3.02), chemical for the precipitation recovery of Li ($0.57), and electricity cost ($0.17). Meanwhile, the product H_2 ($0.014), the disassembled battery units ($0.257), and the final product Li_2CO_3 ($11.06) can well compensate for the input cost of recycling 1.0 kg of $LiFePO_4$ batteries. On the basis of this condition, the calculated profit for the entire process is $5.16, ensuring the economic sustainability of the lithium extraction for $LiFePO_4$ batteries. Moreover, we also further calculated the profit for recycling lithium from 1 kg of spent $LiNi_{0.5}Co_{0.2}Mn_{0.3}O_2$ battery and 1 kg of spent $LiCoO_2$ battery based on our lithium recycling system, which are estimated to be $11.47 (fig. S25) and $11.01 (fig. S26), respectively.

DISCUSSION

In summary, we have demonstrated a nondestructive, green, and high-purity lithium recycling strategy for various spent LIBs including

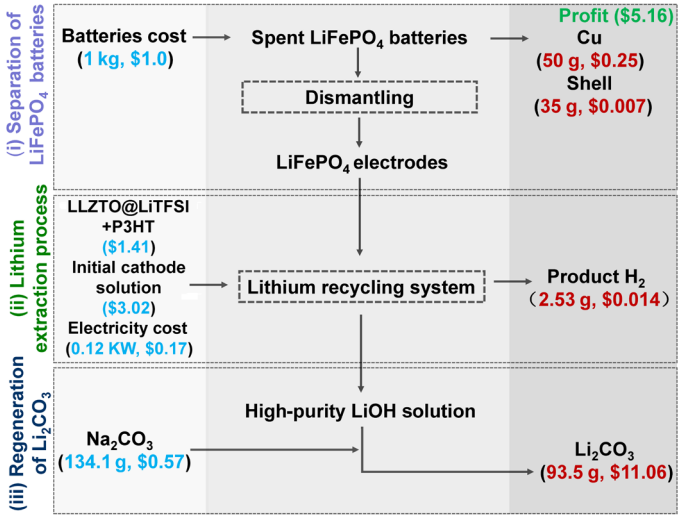

Fig. 6. Cost assessment of the lithium recycling process for spent $LiFePO_4$ battery based on the roll-to-roll system.

$LiFePO_4$, $LiCoO_2$, and $LiNi_{0.5}Co_{0.2}Mn_{0.3}O_2$ based on the proposed "lithium-rich electrode(anode)||LLZTO@P3HT||LiOH(cathode)" system. During the recycling process, the Li^+ from the Li-enriched electrode can be extracted by the high selectivity of LLZTO solid-state electrolyte under the current driven, which can be recovered in the form of LiOH along with the generation of H_2 gas. In addition, modifying LLZTO with LiTFSI+P3HT also successfully extends the range of LLZTO's service environments, particularly in the aqueous solution. LiTFSI+P3HT coating prevents H^+/Li^+ exchange between H_2O and LLZTO. Our rationally designed lithium recycling device has been confirmed to achieve repeatable lithium extraction from various spent LIBs with a recovery rate of 97%. It realizes a technology with low energy consumption and high economic and environmental benefits.

Our approach is completely different from the traditional recycling strategies using hydrometallurgical, pyrometallurgical, and biometallurgy methods (table S4). It achieves high-purity (99%) LiOH enrichment while maximally preserving the electrode integrity for other valuable metal recovery. Our lithium recycling strategy is proven to be a green and sustainable method. The green aspects of our lithium recycling strategy mainly reflect in the following points: (i) The recovery strategy is eco-friendly without using chemicals such as acids and alkalis and eliminates the emission of wastewater and polluting gas. (ii) Our approach directly recycles the waste Li-containing electrode without any pretreatment that require separating cathode materials from the Al foil substrates and organic binders, which avoids the using of organic solvents and additional calcining process to burn off the residues such as carbon and polyvinylidene difluoride, reducing the contamination to the environment. On the other hand, the sustainable features of our lithium recycling method can be traced from the following points: (i) Our method is characterized by minimal water and electricity usage, as well as prevention of the release of polluting gases and waste residues to the environment. (ii) The proposed Li extraction process for spent $LiFePO_4$, $LiCoO_2$, and $LiNi_{0.5}Co_{0.2}Mn_{0.3}O_2$ batteries is proven to be economically feasible, guarantying the sustainability of this strategy. (iii) From the perspective of reuse and recycling activities, the excellent mechanical and thermal stability and good lithium

selectivity of the LLZTO tube improve the overall sustainability and reduce production costs. (iv) Instead of restricting to a certain kind of spent battery, our approach is applicable to various Li-containing cathodes such as $LiFePO_4$, $LiCoO_2$, and $LiNi_{0.5}Co_{0.2}Mn_{0.3}O_2$, which lays a solid foundation for the sustainable development of our approach for future large-scale applications. Therefore, this technique could lead to the development of a promising method to secure the supply of lithium for future energy uses.

MATERIALS AND METHODS

Preparation and characterization of garnet-type LLZTO tubes

The cubic garnet-type $Li_{6.5}La_3Zr_{0.5}Ta_{1.5}O_{12}$ (LLZTO) was obtained by the solid-state reaction of Li_2CO_3 (99.99%, with 30% excess; Sinopharm Chemical Reagent Co. Ltd.), La_2O_3 (99.99%; Sinopharm Chemical Reagent Co. Ltd.), ZrO_2 (99.99%; Aladdin), and Ta_2O_5 (99.99%; Ourchem) powders in stoichiometric ratio. After being fully ground with an agate mortar and pestle, the as-prepared materials were heated at 900°C for 6 hours to decompose the metal salts. Following ball milling with 1.2 wt % of Al_2O_3 for 12 hours, a tube with one closed end was obtained by cold isostatic pressing at 330 MPa for 2 min and then annealed at 1140°C for 16 hours under normal atmosphere while being covered by the same mother powder.

Preparation of pure P3HT film

P3HT polymer with an average molecular weight of 30,000 to 60,000 (CAS: 156074-98-5) were purchased from Xi'an Polymer Light Technology Inc. P3HT powder (30 mg) was dissolved into 3 ml of CS_2 solution (in an airtight container) and stirred for 3 min, and then the mixed solution was dropped onto a glass slide. During the CS_2 evaporation process, P3HT molecules could effectively self-assemble into well-ordered structures through intermolecular interactions. Afterward, immersing the P3HT-coated glass slide into water for 30 min, a pure P3HT film will float on the surface of water because of its hydrophobic nature. The thickness of the yielded film can be well controlled on the basis of the amount of the polymer solution applied.

Preparation of LLZTO@LiTFSI+P3HT

All these processes were conducted in a hooded fume cupboard. Solutions of P3HT and LiTFSI were respectively prepared by dissolving the materials in anhydrous chloroform and anhydrous acetonitrile with a concentration ratio of 8:1 and stirred overnight. P3HT solution was then mixing with LiTFSI solution to achieve P3HT+LiTFSI mixed solution. Then, the LLZTO tube was soaked in the mixed solution for 5 min. Afterward, the LLZTO@LiTFSI+P3HT tube was vertically hung overnight until the solvent volatilized. The thickness of the yielded film is easily controlled on the basis of the amount of the P3HT solution applied. By adjusting the mass of P3HT and LiTFSI in each group, we can obtain the P3HT+LiTFSI films with different thickness.

Preparation of lithium recycling system

LiOH solution (1 M) was placed in the two LLZTO@LiTFSI+P3HT electrolyte tubes as the initial solution for the enrichment and collection of lithium ions. Two platinum electrodes were inserted into the initial solution as the cathode current collectors, which are connected to the negative terminal of the battery test instrument. Copper wire is introduced into the rotating shaft of the motor as the current collector, which is connected with the positive terminal of the battery test machine. The hollow LLZTO is used to selectively extract lithium ion from the spent electrode into the DI water. The wetting lithium-ion electrode passes over the two LLZTO ceramic tubes, so as to ensure the design of double-sided and bidirectional recycling of spent electrode. The operating temperature of this system is set to 50°C to guarantee the excellent Li^+ conductivity of LLZTO. The Li extraction was carried out in the dry box filled with N_2 atmosphere.

The working principle of lithium recycling system

First, valve 1 was opened while valves 2 and 3 remain closed, and the DI water was pumped into the LLZTO@LiTFSI+P3HT solid electrolytes as the initial solution for lithium-ion enrichment. Afterward, valves 2 and 3 were opened, while valve 1 was kept closed. Driven by external electric field, the Li^+ was extracted from the $LiFePO_4$ electrode at the anode side accompanied by the formation of $FePO_4$. Meanwhile, at the cathode, the deionized water is electrolyzed into OH^- and H^+ ions. OH^- combines with the extracted Li^+ to form LiOH. At the same time, H^+ capture electrons from the external circuit, resulting in the generation of H_2 gas, which drives the Li^+ from the spent electrode to be enriched in the cathode compartment through the selectivity of LLZTO@LiTFSI+P3HT. Last, when the charging voltage reached 4.1 V, the battery test machine is stopped. At this moment, valve 2 was opened while valve 1 was closed, and the LiOH reaction liquid in the hollow LLZTO ceramics is effectively recovered into the container under the action of pump.

Materials characterizations

XRD patterns were obtained on a film XRD system (Panalytical X'celerator multielement detector with Cu Kα radiation source, λ = 1.54056 Å). The dynamic water contact angles were measured with a DSA100 instrument. A droplet volume of 3 μl was used for each measurement. The morphologies of the materials were characterized by scanning electron microscopy (ZEISS Ultra 55) with Energy Dispersive Spectrometer mapping. XPS measurement was performed on an ESCALAB250Xi (Thermo Fisher Scientific) with a monochromatic Al Kα source. The lithium content in the electrodes and enriched solution was measured by ICP-OES measurements (Agilent ICP-OES 725 ES). Liquid samples for ICP-OES were diluted with a 1% aqueous nitric acid where necessary, while solid samples were initially dissolved in a small amount of a 70% aqueous nitric acid solution using a digester and then diluted to the required concentration range using a 1% aqueous nitric acid solution. The TOF-SIMS measurements were performed on a PHI nano TOF II with a bismuth liquid metal ion source, and the pressure of the chamber was around 10^{-7} Pa. Sputtering with an Ar ion beam (1 kV and 100 nA) was applied for depth profiling analysis, corresponding to sputtering areas of 400 μm by 400 μm. EIS was conducted on a Bio-Logic VMP3 workstation.

Density functional theory calculations

The first-principles calculations based on the density functional theory were performed using the CASTEP (*43*, *44*). The Perdew-Burke-Ernzerhof exchange-correlation functional within the generalized gradient approximation was used to describe the exchange-correlation energy (*45*). The projector-augmented-wave method was adopted for the pseudopotentials (*46*). The energy cutoff for the plane wave basis expansion was set to 450 eV. The

convergence criteria for total energy and force on each atom were set as 10^{-4} eV and 0.02 eV/Å, respectively. A slab model was constructed with a vacuum layer of 15 Å in the z direction to avoid the interaction between layers. Brillouin zone for LLZTO was set with $3 \times 3 \times 1$ by the Monkhorst-Pack method (*47*), but it is extended to $4 \times 4 \times 4$ for bulk case. The van der Waals interaction has been considered using the Grimme dispersion scheme (*48*). LLZTO was model with a cubic cell $a = b = c = 12.92$ Å, with a formula $Li_{51.20}O_{96}Zr_{11.20}La_{24}Ta_{4.80}$ through factional occupancy, which results in an atom ratio $Li_{6.4}La_3Zr_{1.4}Ta_{0.6}O_{12}$. P3HT was simulated with single-unit $C_{10}H_{16}S$, which is dominated by hydrophobic alkyl. Water adsorption was modeled with $(H_2O)_{12}$ adsorbed on the surface with and without P3HT protection. LLZTO surface was modeled by the 1×1 slab of (010) surface, with a thickness of ~10 Å. Specifically, the slab model contains $Li_{39}O_{72}Zr_9La_{18}Ta_3$, leading to an atomic ratio $Li_{6.5}La_3Zr_{1.5}Ta_{0.5}O_{12}$, being close to experimental result $Li_{6.4}La_3Zr_{1.4}Ta_{0.6}O_{12}$.

SUPPLEMENTARY MATERIALS

Supplementary material for this article is available at https://science.org/doi/10.1126/sciadv.abq7948

REFERENCES AND NOTES

1. D. Lin, Y. Liu, Y. Cui, Reviving the lithium metal anode for high-energy batteries. *Nat. Nanotechnol.* **12**, 194–206 (2017).
2. T. Raj, K. Chandrasekhar, A. N. Kumar, P. Sharma, A. Pandey, M. Jang, B. H. Jeon, S. Varjani, S. H. Kim, Recycling of cathode material from spent lithium-ion batteries: Challenges and future perspectives. *J. Hazard. Mater.* **429**, 128312 (2022).
3. G. Harper, R. Sommerville, E. Kendrick, L. Driscoll, P. Slater, R. Stolkin, A. Walton, P. Christensen, O. Heidrich, S. Lambert, A. Abbott, K. Ryder, L. Gaines, P. Anderson, Recycling lithium-ion batteries from electric vehicles. *Nature* **575**, 75–86 (2019).
4. S. Wang, C. Wang, F. Lai, F. Yan, Z. Zhang, Reduction-ammoniacal leaching to recycle lithium, cobalt, and nickel from spent lithium-ion batteries with a hydrothermal method: Effect of reductants and ammonium salts. *Waste Manag.* **102**, 122–130 (2020).
5. T. C. Wanger, The Lithium future-resources, recycling, and the environment. *Conserv. Lett.* **4**, 202–206 (2011).
6. P. Meshram, B. D. Pandey, T. R. Mankhand, Extraction of lithium from primary and secondary sources by pre-treatment, leaching and separation: A comprehensive review. *Hydrometallurgy* **150**, 192–208 (2014).
7. P. Greim, A. A. Solomon, C. Breyer, Assessment of lithium criticality in the global energy transition and addressing policy gaps in transportation. *Nat. Commun.* **11**, 4570 (2020).
8. H. Vikström, S. Davidsson, M. Höök, Lithium availability and future production outlooks. *Appl. Energy* **110**, 252–266 (2013).
9. C. Liu, Y. Li, D. Lin, P. C. Hsu, B. Liu, G. Yan, T. Wu, Y. Cui, S. Chu, Lithium extraction from seawater through pulsed electrochemical intercalation. *Joule* **4**, 1459–1469 (2020).
10. L. S. Martins, L. F. Guimaraes, A. B. Botelho Junior, J. A. S. Tenorio, D. C. R. Espinosa, Electric car battery: An overview on global demand, recycling and future approaches towards sustainability. *J. Environ. Manage.* **295**, 113091 (2021).
11. K. Kim, D. Raymond, R. Candeago, X. Su, Selective cobalt and nickel electrodeposition for lithium-ion battery recycling through integrated electrolyte and interface control. *Nat. Commun.* **12**, 6554 (2021).
12. C. Liu, J. Lin, H. Cao, Y. Zhang, Z. Sun, Recycling of spent lithium-ion batteries in view of lithium recovery: A critical review. *J. Clean. Prod.* **228**, 801–813 (2019).
13. H. Bae, Y. Kim, Technologies of lithium recycling from waste lithium ion batteries: A review. *Mater. Adv.* **2**, 3234–3250 (2021).
14. J. Piątek, S. Afyon, T. M. Budnyak, S. Budnyk, M. H. Sipponen, A. Slabon, Sustainable Li-Ion batteries: Chemistry and recycling. *Adv. Energy Mater.* **11**, 2003456 (2020).
15. A. Battistel, M. S. Palagonia, D. Brogioli, F. La Mantia, R. Trocoli, Electrochemical methods for lithium recovery: A comprehensive and critical review. *Adv. Mater.* **32**, e1905440 (2020).
16. B. Swain, Recovery and recycling of lithium: A review. *Sep. Purif. Technol.* **172**, 388–403 (2017).
17. A. B. Botelho Junior, S. Stopic, B. Friedrich, J. A. S. Tenório, D. C. R. Espinosa, Cobalt recovery from Li-Ion battery recycling: A critical review. *Metals* **11**, (2021).
18. X. Zhang, L. Li, E. Fan, Q. Xue, Y. Bian, F. Wu, R. Chen, Toward sustainable and systematic recycling of spent rechargeable batteries. *Chem. Soc. Rev.* **47**, 7239–7302 (2018).
19. B. Makuza, Q. Tian, X. Guo, K. Chattopadhyay, D. Yu, Pyrometallurgical options for recycling spent lithium-ion batteries: A comprehensive review. *J. Power Sources* **491**, 229662 (2021).
20. L. F. Guimaraes, A. B. Botelho Junior, D. C. R. Espinosa, Sulfuric acid leaching of metals from waste Li-ion batteries without using reducing agent. *Miner. Eng.* **183**, 107597 (2022).
21. W. Lv, Z. Wang, H. Cao, Y. Sun, Y. Zhang, Z. Sun, A critical review and analysis on the recycling of spent Lithium-Ion batteries. *ACS Sustain. Chem. Eng.* **6**, 1504–1521 (2018).
22. Y. Yao, M. Zhu, Z. Zhao, B. Tong, Y. Fan, Z. Hua, Hydrometallurgical processes for recycling spent Lithium-Ion batteries: A critical review. *ACS Sustain. Chem. Eng.* **6**, 13611–13627 (2018).
23. M. K. Tran, M.-T. F. Rodrigues, K. Kato, G. Babu, P. M. Ajayan, Deep eutectic solvents for cathode recycling of Li-ion batteries. *Nat. Energy* **4**, 339–345 (2019).
24. D. Mishra, D. Kim, D. Ralph, J. Ahn, Y. Rhee, Bioleaching of metals from spent lithium ion secondary batteries using *Acidithiobacillus ferrooxidans*. *Waste Manag.* **28**, 333–338 (2008).
25. H. Bae, S. M. Hwang, I. Seo, Y. Kim, Electrochemical Lithium recycling system toward renewable and sustainable energy technologies. *J. Electrochem. Soc.* **163**, E199–E205 (2016).
26. Y. Li, W. Lv, H. Huang, W. Yan, X. Li, P. Ning, H. Cao, Z. Sun, Recycling of spent lithium-ion batteries in view of green chemistry. *Green Chem.* **23**, 6139–6171 (2021).
27. A. J. Samson, K. Hofstetter, S. Bag, V. Thangadurai, A bird's-eye view of Li-stuffed garnet-type $Li_7La_3Zr_2O_{12}$ ceramic electrolytes for advanced all-solid-state Li batteries. *Energ. Environ. Sci.* **12**, 2957–2975 (2019).
28. C. Wang, W. Ping, Q. Bai, H. Cui, R. Hensleigh, R. Wang, A. H. Brozena, Z. Xu, J. Dai, Y. Pei, C. Zheng, G. Pastel, J. Gao, X. Wang, H. Wang, J. C. Zhao, B. Yang, X. (R.) Zheng, J. Luo, Y. Mo, B. Dunn, L. Hu, A general method to synthesize and sinter bulk ceramics in seconds. *Science* **368**, 521–526 (2020).
29. J. Xu, K. Liu, Y. Jin, B. Sun, Z. Zhang, Y. Chen, D. Su, G. Wang, H. Wu, Y. Cui, A garnet-type solid-electrolyte-based molten Lithium–Molybdenum–Iron(II) chloride battery with advanced reaction mechanism. *Adv. Mater.* **32**, e2000960 (2020).
30. R. Murugan, V. Thangadurai, W. Weppner, Fast lithium ion conduction in garnet-type $Li_7La_3Zr_2O_{12}$. *Angew. Chem. Int. Ed. Engl.* **46**, 7778–7781 (2007).
31. J. G. Connell, T. Fuchs, H. Hartmann, T. Krauskopf, Y. Zhu, J. Sann, R. Garcia-Mendez, J. Sakamoto, S. Tepavcevic, J. Janek, Kinetic versus thermodynamic stability of LLZO in contact with Lithium metal. *Chem. Mater.* **32**, 10207–10215 (2020).
32. C. Wang, K. Fu, S. P. Kammampata, D. W. McOwen, A. J. Samson, L. Zhang, G. T. Hitz, A. M. Nolan, E. D. Wachsman, Y. Mo, V. Thangadurai, L. Hu, Garnet-type solid-state electrolytes: Materials, interfaces, and batteries. *Chem. Rev.* **120**, 4257–4300 (2020).
33. Y. Shimonishi, A. Toda, T. Zhang, A. Hirano, N. Imanishi, O. Yamamoto, Y. Takeda, Synthesis of garnet-type $Li_{7-x}La_3Zr_2O_{12-1/2x}$ and its stability in aqueous solutions. *Solid State Ion.* **183**, 48–53 (2011).
34. Y. Li, J.-T. Han, S. C. Vogel, C.-A. Wang, The reaction of $Li_{6.5}La_3Zr_{1.5}Ta_{0.5}O_{12}$ with water. *Solid State Ion.* **269**, 57–61 (2015).
35. C. Galven, J. Dittmer, E. Suard, F. Le Berre, M.-P. Crosnier-Lopez, Instability of Lithium garnets against moisture. Structural characterization and dynamics of $Li_{7-x}H_xLa_3Sn_2O_{12}$ and $Li_{5-x}H_xLa_3Nb_2O_{12}$. *Chem. Mater.* **24**, 3335–3345 (2012).
36. H. Huo, J. Luo, V. Thangadurai, X. Guo, C.-W. Nan, X. Sun, Li_2CO_3: A critical issue for developing solid garnet batteries. *ACS Energy Lett.* **5**, 252–262 (2020).
37. J. F. Wu, B. W. Pu, D. Wang, S. Q. Shi, N. Zhao, X. Guo, X. Guo, In situ formed shields enabling Li_2CO_3-free solid electrolytes: A new route to uncover the intrinsic lithiophilicity of garnet electrolytes for dendrite-free Li-metal batteries. *ACS Appl. Mater. Interfaces* **11**, 898–905 (2019).
38. M. Matsui, K. Sakamoto, K. Takahashi, A. Hirano, Y. Takeda, O. Yamamoto, N. Imanishi, Phase transformation of the garnet structured lithium ion conductor: $Li_7La_3Zr_2O_{12}$. *Solid State Ion.* **262**, 155–159 (2014).
39. A. Paolella, W. Zhu, G. Bertoni, S. Savoie, Z. Feng, H. Demers, V. Gariepy, G. Girard, E. Rivard, N. Delaporte, A. Guerfi, H. Lorrmann, C. George, K. Zaghib, Discovering the influence of Lithium loss on garnet $Li_7La_3Zr_2O_{12}$ electrolyte phase stability. *ACS Appl. Energy Mater.* **3**, 3415–3424 (2020).
40. J. Lang, Y. Jin, K. Liu, Y. Long, H. Zhang, L. Qi, H. Wu, Y. Cui, High-purity electrolytic lithium obtained from low-purity sources using solid electrolyte. *Nat. Sustain* **3**, 386–390 (2020).
41. Y. Park, N. H. Kim, J. M. Kim, Y. C. Kim, Y. U. Jeong, S. M. Lee, H. C. Choi, Y. M. Jung, Surface reaction of $LiCoO_2$/Li system under high-voltage conditions by X-ray spectroscopy and two-dimensional correlation spectroscopy (2D-COS). *Appl. Spectrosc.* **65**, 320–325 (2011).
42. L. Dahéron, R. Dedryvère, H. Martinez, M. Ménétrier, C. Denage, C. Delmas, D. Gonbeau, Electron transfer mechanisms upon lithium deintercalation from $LiCoO_2$ to CoO_2 investigated by XPS. *Chem. Mater.* **20**, 583–590 (2008).
43. S. J. Clark, M. D. Segall, C. J. Pickard, P. J. Hasnip, M. I. J. Probert, K. Refson, M. C. Payne, First principles methods using CASTEP. *Zeitschrift für Kristallographie – Crystal. Mater.* **220**, 567–570 (2005).
44. E. R. McNellis, J. Meyer, K. Reuter, Azobenzene at coinage metal surfaces: Role of dispersive van der Waals interactions. *Phys. Rev. B* **80**, 205414 (2009).
45. J. P. Perdew, J. A. Chevary, S. H. Vosko, K. A. Jackson, M. R. Pederson, D. J. Singh, C. Fiolhais, Atoms, molecules, solids, and surfaces: Applications of the generalized gradient approximation for exchange and correlation. *Phys. Rev. B Condens. Matter* **46**, 6671–6687 (1992).

46. P. E. Blochl, Projector augmented-wave method. *Phys. Rev. B Condens. Matter* **50**, 17953–17979 (1994).
47. H. J. Monkhorst, J. D. Pack, Special points for Brillouin-zone integrations. *Phys. Rev. B* **13**, 5188–5192 (1976).
48. S. Grimme, J. Antony, S. Ehrlich, H. Krieg, A consistent and accurate ab initio parametrization of density functional dispersion correction (DFT-D) for the 94 elements H-Pu. *J. Chem. Phys.* **132**, 154104 (2010).

Acknowledgments: We thank X. Zhang from the Zhengzhou University for experiment discussion and suggestion. **Funding:** J.X. acknowledges support by the National Natural Science Foundations of China Grant (5200235), China Postdoctoral Science Foundation Grants (2020 T130615 and 2019 M662523). H.T. was supported by the Interdisciplinary Innovation Program of North China Electric Power University (XM2212315). **Author contributions:** Conceptualization: J.X., Y.J., and K.L. Methodology: J.X., H.L., and H.T. Investigation: Z.Z., B.S., and Q.J. Visualization: N.L. Supervision: G.W., M.A., H.W., and M.L. Writing—original draft: J.X. Writing—review and editing: M.A., D.S., and X.G. **Competing interests:** The authors declare that they have no competing interests. **Data and materials availability:** All data needed to evaluate the conclusions in the paper are present in the paper and/or the Supplementary Materials.

Submitted 4 May 2022
Accepted 18 August 2022
Published 5 October 2022
10.1126/sciadv.abq7948